Construction and Building Materials 448 (2024) 138230

Contents lists available at ScienceDirect

Construction and Building Materials

journal homepage: www.elsevier.com/locate/conbuildmat

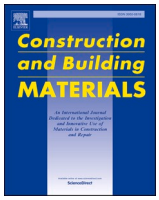

Use of multivariate clustering analysis to investigate the physicochemical interactions in bitumen mastics using micromechanical modeling and FTIR spectroscopy

Seyed Mohsen Motevalizadeh [*,1], Konrad Mollenhauer

Engineering and Maintenance of Road Infrastructure, Faculty of Civil and Environmental Engineering, University of Kassel, Kassel, Germany

ARTICLE INFO

Keywords:
Micromechanical modeling
Physicochemical interactions
Adsorbed interphase layer
Warm mix asphalt
Foamed bitumen

ABSTRACT

The debate continues regarding whether different mineral fillers and asphalt technologies mitigate or accelerate aging formation in bituminous mastics. Hence, this study was centered on investigating the concurrent impact of aging stages, mineral composition of filler components (e.g., limestone, basalt, and diabase), and asphalt binder technology on the formation and evolution of physicochemical interactions in bituminous mastics. Various bituminous mastics at different aging stages were analyzed using rheological oscillatory testing and Attenuated Total Reflectance Fourier Transform Infrared spectroscopy (ATR-FTIR) measurements to study their chemical characteristics. A generalized self-consistent scheme (GSCS) and Hashin micromechanical models were utilized to estimate immobilized binder volume and adsorbed binder thickness values from rheological data. Additionally, aging-related indices such as carbonyl and sulfoxide indices were calculated from FTIR-ATR results. In addition to the typical comparison of these results, a multivariate clustering approach was employed, comprising Partial Least-Square Regression (PLSR) as a dimensionality reduction protocol and Hierarchical Clustering Analysis (HCA) as a clustering technique. This approach segregated the mastics into four distinct clusters without prior knowledge of their labels. The clustering results grouped variants with similar physicochemical attributes in specific clusters, revealing the mitigating role of various filler types based on the dominant components of each cluster. Based on the physicochemical results obtained from the clustering analysis, limestone filler is expected to play a more significant mitigating role in foamed bitumen mastics, helping to alleviate the effects induced by aging protocols.

1. Introduction

The aging dynamics within asphalt mixtures are shaped not only by the inherent characteristics of the asphalt binder but also by the chemical composition and properties of attributes of the added fillers [1]. Given that aging primarily occurs at the interface of the binder and mineral constituents within the asphalt mix, a comprehensive understanding can be attained through an examination of the composite structure of binder and mineral components. This composite framework, referred to as bituminous mastics, forms the macrostructure of asphalt.

Bituminous mastics exhibited a stronger correlation with asphalt mixture performance compared to asphalt binder alone [2]. The effectiveness of bituminous mastics relies heavily on the reinforcing mechanisms of the fillers [3,4], which can be classified into three primary scenarios: (i) volume filling, (ii) particle structurization, and (iii) physicochemical interactions. The first two scenarios involve mechanical reinforcement, addressable based on mechanical behaviors, while the third necessitates investigation with higher resolution. Physically reinforcing mechanisms impact aging by mitigating oxygen diffusion, while physicochemical interactions influence the aging process by affecting the adsorbed interphase layer [1]. Physical reinforcement primarily relies on the stiffening effect of mineral fillers on the composite structure of bituminous mastics, leading to an increase in viscosity. In contrast, physicochemical reinforcement is governed by interfacial interactions between the bitumen and mineral components, influenced by the mineralogical and physical properties of reinforcing constituents [1]. Notably, fillers play a more substantial role in shaping the physicochemical interactions in asphalt mixtures than coarser aggregates,

* Corresponding author.
E-mail address: m.motevalizadeh@uni-kassel.de (S.M. Motevalizadeh).
[1] https://orcid.org/0000-0001-8304-6271

https://doi.org/10.1016/j.conbuildmat.2024.138230
Received 7 March 2024; Received in revised form 26 July 2024; Accepted 3 September 2024
Available online 9 September 2024

attributed to their larger surface areas and increased interfacial interactions.

Adsorption, a crucial process involving bitumen and mineral components, anchors the polar elements of the binder onto the filler surface [1]. Asphaltenes, highly polar constituents of bitumen, stand in contrast to resins, aromatics, and saturates, which are considered less and non-polar [5]. Moraes et al. [5] highlighted that the adsorption process plays a mitigating role in aging evolution, countering the catalyzing role of mineral components in fillers. The extent to which various mineral compositions and components affect bitumen oxidation has been a subject of debate. Additionally, it is noteworthy to mention that the chemical and physical components of the adsorbed binder layer differ from those in the bulk asphalt binder [6]. In simpler terms, the aging mechanism in bituminous mixtures is intricately governed by the characteristics of the asphalt binder, mineral components, and the molecular interaction between the two components.

Beyond known factors affecting aging, the role of mineral components can be analyzed based on polar fractions. Higher adsorption capability results in lower oxidation intensities. Understanding the structure of the asphalt constituent fractions and their dependency on the presence of fillers is beneficial in this context. Asphaltene molecules, surrounded by the resins, constitute the dispersed phase, while saturates and aromatics form the continuous phase. Incorporation of mineral filler particles subsequently changes the distribution of these phases, altering the characteristics of the asphalt binder [7]. On the other hand, it was discovered that filler concentrations significantly affect the stiffening mechanisms, transitioning from physical reinforcement to physicochemical and particle interaction effects [8]. Given that effective filler concentration in asphalt mixtures varies between 20 % and 45 % by volume [7], and filler particle interaction effects are expected at concentrations greater than 40 % (by volume) [9], physicochemical interfacial interaction between filler and binder dominates the stiffening in asphalt structure. This effect can be explained by binder adsorption to the aggregate surface, significantly dependent on filler concentration, surface area, and composition.

Distinguishing asphalt binder based on the polarity levels yields four major fractions termed SARA (Saturates, Aromatics, Resins, Asphaltene) fractions, where increased molecular polarity increases the binder stiffness [10]. This concept, the relationship between the molecular polarity and stiffness, can be therefore used to explain the mechanism of bitumen-filler interaction by distinguishing between the adsorbed (structural) and bulk (free) bitumen components in the presence of filler particles. Guo et al. [11] differentiated between the structural and free bitumen components in the bitumen-filler structure, confirming that the complex shear modulus of structural bitumen was larger due to the presence of stiff and polar molecules like asphaltenes and resins. This observation by Guo et al. [11] confirmed that molecules with higher polarity levels were more readily adsorbed onto the surface of mineral filler particles. On the other hand, the use of various asphalt mix technologies significantly changes the polarity level and consequently alters the interfacial physicochemical interaction in the bitumen-filler structure.

Foam bitumen technology, a method to produce asphalt mixes at lower mixing temperatures can cover a wide range of mixing protocols consisting of warm mix asphalt (WMA), half-warm mix asphalt, and cold mix asphalt pavements [12–14]. Among the possibilities to produce foamed bitumen, the water-based foaming technique can cause changes in the engineering properties of bituminous mixtures categorized into (i) the physical changes in bitumen structure, (ii) chemical interactions with mineral components, and (iii) physical interactions between water, pressured air, and bitumen. The use of the foamed WMA technique reduces the challenges regarding short-term aging despite the increased concerns regarding the experience of moisture damage [15]. Studying the impact of the foaming process on the bitumen's chemistry denied any significant relationship [16]; similarly, that impact on the microstructure of the product was noticed as negligible [17]. It also resolved the concerns over the detrimental effects of foaming on the high-temperature rheological and functional responses of foam bitumen [18,19], explained by the treating effect of exposure to high temperatures. Despite these promises, some concerns remain over the consequences of the multiphase structure of a foam system. Maciejewski al. [20] discussed this issue by analyzing the asphalt volumetric characteristics and changes in binder film thickness. Similarly, the infusion rate of water into the bitumen and the consequent impact on the bitumen's molecular structure was assessed [21]. This investigation revealed evidence of chemical conversions and changes in bitumen microstructure.

The intricate role of mineral fillers in shaping the physicochemical interactions in the asphalt composite structure, coupled with intrinsic characteristics of foamed-bitumen technology results in highly complex behavior. Indeed, by increasing the use of WMA mixes in asphalt road surfacing, the aging-induced stiffening and subsequent distresses will be altered compared to what is expected from traditional hot asphalt mixtures. Given the lack of extensive knowledge in explaining the exact role of mineral fillers in inducing physicochemical interactions, the application of various asphalt production technologies with ambiguous impacts on the binder polarity increases the level of uncertainty. In particular, use of water-based foamed bitumen technology which directly injects water contents into the asphalt binder makes it more challenging to predict the asphalt aging intensity. Hence, going in-depth into the concept of physical and interfacial physicochemical reinforcements in foamed bitumen mastics will shed light on more scientific insights into aging evolution.

The micromechanical modeling approach showed promise in analyzing the reinforcing mechanisms in bituminous mastics caused by the incorporation of mineral fillers. Considering asphalt mixture as a composite media, linear viscoelastic characteristics can be approximated by assuming distinctive subphases, even though it is challenging to predict the composite modulus of bituminous mastics based on the characteristics of constituents (i.e., the proportion of the phases and moduli of each). To overcome this shortcoming, several micromechanical models have been proposed relying on the assumption that asphalt composites exhibit a multiphase structure [22]. In this context, the self-consistent model, generalized self-consistent scheme, Mori-Tanka scheme, and Phy-C models were previously proposed to estimate the complex modulus of the overall complex medium and the constituent phases. These models can be categorized based on those of principal assumptions into multiphase models; to what extent considering the interfacial physicochemical interactions. Indeed, ignoring the physicochemical interactions may cause a notable underestimation in approximating the viscoelastic responses of bituminous mastics since higher values of fillers' specific area, compared to those of mineral aggregates, catalyze the physicochemical interactions at the interface of filler-binder. To address this latter shortcoming, the researchers attempted to consider some modifications to the precedent models; Buttlar et al. [23] modified the GSCS model by approximating the effective volume of filler particles. Another effective approach was also replacing the filler concentration in Hashin and Shtrikman [24] model by the effective filler fractions [25]. Further, Underwood et al. [22] developed a four-phase micromechanical model, termed Phy-C, relying on the general formulation of Herve and Zaoui [26] by assuming that the filler (inclusion) is coated with numerous layers which can be an illustration of physicochemical interactions and asphalt binder adsorption. Another form of GSCS, a two-phase model introduced by Christensen and Lo [27], offers promises in elucidating the bitumen absorbance process over mineral particle surfaces when the particle fraction is low enough, typically around 25 %. However, as the filler volume fraction surpasses this threshold, these models lose efficiency in predicting the linear viscoelastic behavior of mastics. The reinforcement effect of filler particles becomes underestimated in such scenarios. It's important to highlight that beyond the intended aim of employing micromechanical models to predict the complex modulus of the composite, additional insights into the characteristics of adsorbed binders can be obtained.

This includes determining the volume of the immobilized binder through the GSCS model [28] and estimating the thickness of the adsorbed binder using the Hashin model.

Within this context, assessing the impact of various filler types on the aging evolution in water-based foamed WMA bituminous mastics given the notable role of interactions between binder and mineral fillers in the aging evolution [29]. By determining different aspects of material characteristics, a general pattern behind aging evolution was searched relying on the rheological and chemical characteristics of bituminous mastics. The ultimate objectives of this research are as follows:

(i) Exploring the role of mineral fillers on the adsorbed interphase layer and mastic microstructure,
(ii) Assessing the physicochemical interaction between mineral fillers and foamed bitumen using calculating the interfacial adsorbed film thickness and volume of immobilized binder volume,
(iii) Elucidating the latent role of the aging process on the physicochemical and chemical characteristics of bituminous mastics

2. Research approach

This research paper is focused on exploring the evolution of aging in bituminous mastics by characterizing the physicochemical interaction between asphalt binders and mineral components. To this end, bituminous mastics were studied by incorporating three different filler types into bitumen after those exposed to various aging protocols. The mastics were examined by performing the oscillatory tests using dynamic shear rheometer and the derived complex shear moduli were analyzed by means of time-temperature superposition principle, generalized self-consistent scheme (GSCS) and Hashin micromechanical models. The chemical characteristics of the bituminous mastics were also assessed through the Fourier Transform Infrared (FTIR) spectroscopy test. The aim was to distinguish the significance of the filler's mineral composition and the bitumen aging stage on the formation of adsorbed binder components in bituminous mastics.

3. Materials and method

Unmodified bitumen with a penetration grade of 50/70 was used in this research as the base binder to produce the water-based foamed bitumen using Wirtgen WLB-10S laboratory scale plant. The foamed bitumen production was initiated by determining the optimum water content equal to 2.9 % according to the process outlined in [12,30–32]. To fabricate the desired bituminous mastics, three filler types with the specific gravity of 2.851 g/cm^3, 3.184 g/cm^3, and 2.695 g/cm^3 for limestone, basalt, and diabase filler, respectively, were incorporated maintaining the constant volumetric concentration of 27 %. Maintaining this volumetric concentration in all the mastic variants, which was taken following the suggestion of [33], eliminates the contribution of particle reinforcing phenomenon from the mechanical and rheological responses. Further characteristics of mineral fillers including filler-specific surfaces and ΔR&B (DIN EN: 13179-1) have been measured as reported in Table 1. It should be mentioned that the ΔR&B testing has been conducted by employing 50/70 Pen bitumen for the sake being consistent with the testing program. A detailed process of the mastic mixing design can be reached in [28,33]. The components and the corresponding volumetric composition of four desired mastic variants are illustrated in Table 1.

The mastics were generated by heating the mineral fillers for 6 h at 160 °C and added to the foamed bitumen 60 min after the foaming process. The mastics were mixed for 20 min using a low-shear mixing device. It is important to note that during mastic preparation, the fillers were added to the foam bitumen and virgin bitumen at temperatures of 130 °C and160 °C, respectively. To proceed with the experimental program, the generated mastics underwent laboratory short-term and long-term aging procedures relying on the Rolling Thin Film Oven Test (RTFOT) and Pressure Aging Vessel (PAV) protocols proposed by ASTM D 2872 and ASTM D 6521, respectively.

The mastic variants at various aging levels as well as the water-based foam bitumen and base binder were characterized in the linear viscoelastic domain by subjecting to the temperature-frequency sweep (TFS) test. TFS testing was carried out using a dynamic shear rheometer (Anton Paar Physica MCR 302) by setting the temperatures ranging between −8 °C and 88 °C, with the 6°C increments, and applying nine various angular frequencies (with a logarithmic ramp) varying between 1 rad/s to 100 rad/s. Two parallel geometries of 25 mm, for the temperatures comprising 34 °C to 88 °C, and 8 mm, for the temperatures comprising 34 °C to −8 °C, were employed to implement the TFS testing. To ensure avoiding the lateral impact of testing and/or operational errors, two replicates were performed for each variant.

To analyze the chemical composition of each mastic, the Attenuated Total Reflection Fourier-Transformation Infrared (ATR-FTIR) spectroscopy was conducted by employing a Bruker Alpha device equipped with an attenuated total reflection unit. The spectral wave numbers were targeted ranging from 4000 to 400 cm^{-1} with 24 scans performed for each spectrum. To ensure the reproducibility of the observations and avoid any bias in observations five samples (droplets) were prepared for each testing variant, and each sample was examined five times. The testing was conducted per the protocol provided by Ref. [34].

The aging evolution in bituminous mastics with different mineral components has been investigated in another study [35] using multivariate discriminant analysis. Consequently, these discussions are omitted here for brevity.

4. Formal analyses

4.1. Raw data analysis

The raw data collected from TFS tests were utilized to construct the Black and Cole-Cole diagrams, as depicted in Fig. 1, serving two primary purposes: validating the applicability of the time-temperature superposition (TTS) principle and examining the linear viscoelastic characteristics of the mastics. Fig. 1 compares the findings from unaged control mastic (CM) with those from CM mastics subjected to both RTFOT and PAV aging protocols. For the sake of brevity, the results of additional mastics were excluded. As discerned from Fig. 1, all mastics displayed continuous singular curves, affirming the integrity of the TTS principle [28]. The influence of various filler types appeared negligible on the Black and Cole-Cole diagrams of unaged and RTFOT-aged mastics,

Table 1
Mastics compositions.

Filler type	Binder type	Mastic ID	Filler Specific gravity (g/cm3)	Filler specific surface (cm^3/g)	ΔR&B 50/70 Pen	Binder Mass (g)	Filler Mass (g)	Filler to binder volume ratio
Limestone	Virgin 50/70 bitumen	CM	2.815	5030	15.5	500	518	27 %
Limestone	Foamed bitumen	LM	2.815	5030	15.5		518	
Basalt	Foamed bitumen	BM	3.148	3985	31		580	
Diabase	Foamed bitumen	DM	2.695	5210	12		490	

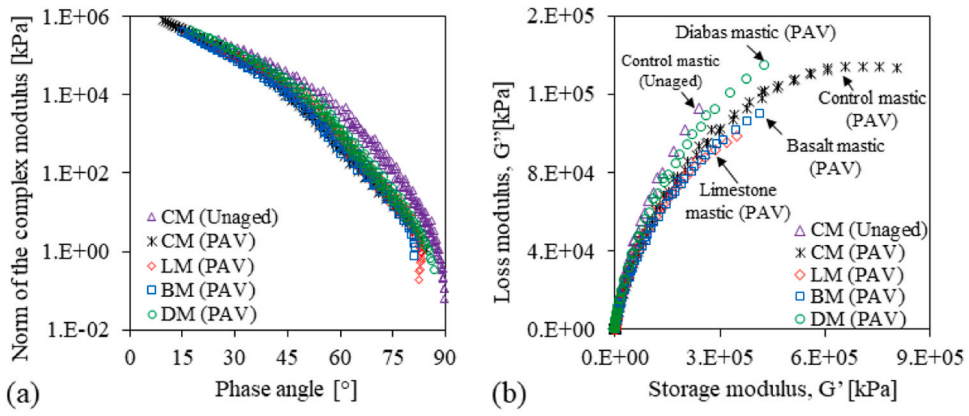

Fig. 1. Representation of the mastics raw data: (a) Black and (b) Cole-Cole diagrams.

whereas the distinct fillers' significance became apparent after exposure to long-term aging.

Analyzing the TFS results revealed a characteristic transition in the curve associated with base bitumen and foam bitumen from a glassy to a viscous state, with the complex shear modulus values decreasing as the phase angle magnitude increased until reaching 90°. Meanwhile, the role of foaming technology in shaping the rheological responses of mastics in the presence of different filler types was investigated, illustrating the minimal impact of bitumen technology on the time-temperature-dependent responses of bituminous mastics when limestone filler is incorporated. In terms of aging, it can be concluded that implementation of aging protocols in bituminous mastics led to more elastic responses with a higher proportion of stored energy compared to dissipated energy.

Examining the impact of fillers on aging-induced stiffening revealed distinct responses. For instance, the presence of diabase fillers exhibited the least changes in material elasticity after exposure to aging protocols, while the presence of basalt filler recorded the most significant change in the black area. Additionally, analysis of raw data based on the Cole-Cole diagram indicated that different filler types and bitumen technology induced changes in both loss and storage moduli. Particularly in long-term aged mastics, the use of foamed bitumen instead of neat bitumen in the presence of limestone, decreased the storage and loss moduli at low temperatures (and/or high frequencies), while the incorporation of diabase filler resulted in higher moduli compared to limestone and basalt fillers. This suggests that in long-term aged mastics, the use of foamed bitumen shifted the Cole-Cole diagrams leftward (lower storage modulus values), indicating a shift towards less elastic responses. In terms of filler types, the degree of aging-induced elasticity can be correlated with limestone, basalt, and diabase, respectively.

To quantify these observations, normalized |G*| and δ values were calculated based on the values associated with unaged mastics as reported in Tables 2 and 3. Following the methodology outlined in [28], these values were determined at an angular frequency of 10 rad/s and temperatures of 4°C, 22°C, 58°C, and 82°C. The results demonstrated an increase in the normalized |G*| and a decrease in the normalized δ due to various aging protocols. Notably, normalized |G*| values for mixes exposed to RTFOT+PAV were significantly higher than those for RTFOT aging alone. Moreover, the impact of aging was more pronounced at higher temperatures than at lower temperatures. Conversely, phase angle values were notably reduced due to aging protocols, with aging accumulation leading to an intense reduction in phase angle. Contrary to the normalized |G*| observations, normalized δ values experienced greater changes at lower temperatures, aligning with previous research on reclaimed asphalt pavement fillers in bituminous mastics [28] and the analysis of aging in bitumen [36].

Beyond aging intensity and temperatures, various filler components can alter material rheological responses. The presented results in Tables 2 and 3 indicate that incorporating foamed bitumen instead of base bitumen mitigated the evolution of aging-induced stiffness. Specifically, lower normalized |G*| ratios and higher normalized δ ratios were observed in mastics incorporating foamed bitumen. Concerning filler types, foamed bitumen mastics with diabase filler exhibited highly significant mitigation effects, while limestone filler mitigated rheological changes, particularly at higher temperatures. Consequently, the impact of filler types and bitumen technology can significantly influence the overall linear viscoelastic responses of aged bituminous mastics.

4.2. Master curves

The Christensen, Anderson, and Marasteanu (CAM) model, along with the Williams-Landel-Ferry (WLF) model, was employed to derive master curves of the complex shear modulus (|G*|) and phase angle (δ) by applying the time-temperature superposition principle [37,38]. This involved determining the reduced frequency (ω_R) based on the actual angular frequency and shift factor. To accurately determine the shift factor, the WLF model was utilized, which integrates the effects of both time and temperature into a master curve, as represented in Eq. (1). In this equation, C_1 and C_2 were utilized to tailor the shift factor for optimal fitting [39].

$$\log(a_T) = -\frac{C_1(T - T_{ref})}{(C_2 + T - T_{ref})} \tag{1}$$

The CAM model was introduced as a mathematical framework to generate master curves of asphalt binders using Eqs. (2) and (3).

$$|G^*|(\omega_r) = |G^*|_g \left[1 + \left(\frac{\omega_c}{\omega_r}\right)^v\right]^{\frac{-m}{v}} \tag{2}$$

$$\delta(\omega_r) = \frac{90.\mathrm{m}}{\left[1 + \left(\frac{\omega_r}{\omega_c}\right)\right]^v} \tag{3}$$

where $G^*(\omega)$ is the complex shear modulus; |G*|g is the glassy dynamic modulus; ω_r is the reduced frequency (rad/sec) at the defined temperature; and ω_c is cross-over frequency (rad/sec) at the defined temperature. Additionally, v and m (where m=log(2)/R) are the dimensionless shape parameters that are obtained through the optimization process. The CAM model (Fig. 2) is formulated as a function of glassy modulus, the rheological index (R), and the crossover frequency. Among these, the crossover frequency characterizes the overall stiffness of bituminous mastics, which increases with decreased ω_c. Moreover, the rheological index is utilized to delineate the transition of bituminous materials from elastic behavior to steady-state flow. Higher magnitudes of rheological index denote less brittle (more elastic behavior) materials under intermediate loading rates and temperatures. Table 4 represents the

Table 2
Normalized |G*| ratios of mastics.

	Angular frequency	CM			LM			BM			DM		
		Unaged |G*| [kPa]	RTFOT	RTFOT+PAV	Unaged |G*| [kPa]	RTFOT	RTFOT+PAV	Unaged |G*| [kPa]	RTFOT	RTFOT+PAV	Unaged |G*| [kPa]	RTFOT	RTFOT+PAV
4 °C	10 rad/s	121,750	1.18	2.32	108,305	1.25	1.48	164,345	0.95	1.15	144,605	0.97	1.06
22 °C		7929.45	1.39	5.99	6574.5	1.56	3.48	12,130.5	0.99	2.13	10,836.5	0.99	1.09
58 °C		19.59	1.81	18.47	19.09	1.75	2.38	27.39	1.42	8.11	24.50	1.35	4.83
82 °C		1.09	1.33	16.79	1.09	1.28	2.47	1.47	1.11	7.32	1.32	1.06	4.52

Table 3
Normalized δ ratios of mastics.

	Angular frequency		CM		LM			BM			DM		
		Unaged δ	RTFOT	RTFOT+PAV	Unaged δ	RTFOT	RTFOT+PAV	Unaged δ	RTFOT	RTFOT+PAV	Unaged δ	RTFOT	RTFOT+PAV
4 °C	10 rad/s	32.60	0.94	0.60	34.045	0.91	0.72	30.02	1.01	0.75	30.09	1.02	0.94
22 °C		55.38	0.93	0.63	56.77	0.91	0.75	53.675	0.97	0.74	53.02	0.98	0.91
58 °C		80.94	0.95	0.75	81.26	0.94	0.89	80.5	0.96	0.79	80.59	0.96	0.84
82 °C		87.89	0.99	0.85	87.95	0.98	0.93	87.73	0.99	0.88	87.79	0.99	0.92

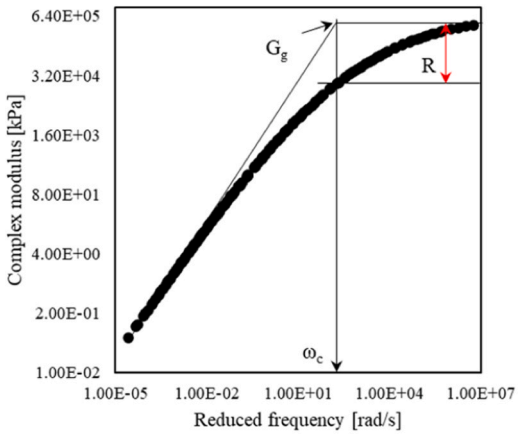

Fig. 2. CAM model parameters.

coefficients obtained from the fitting of CAM model.

Fig. 3 illustrates the master curve of complex modulus and phase angle of the mastics at the reference temperature of 25 °C. To enhance clarity and conciseness, the master curves of PAV-aged mastics were separated from other aging levels. It is noteworthy that the implementation of RTFOT and PAV aging protocols resulted in progressive changes in the rheological responses of different bituminous mastics. Conversely, the influence of aging intensity on the rheological characteristics of various bituminous fillers can be attributed to the filler type and binder technology. Figs. 3a and 2b signified that the incorporation of mineral fillers led to increased stiffness and elasticity of the mastics. Similarly, the impact of sequential aging protocols is evident, demonstrating that higher aging levels correlate with increased stiffness and elasticity across the entire range of reduced frequencies. This observation aligns with the preliminary analysis of the raw data. To distinctly observe the impact of PAV aging on the rheological responses of the bituminous mastics, the master curves of complex modulus and phase angle of PAV-aged mastics were plotted in Figs. 3c and 2d. These curves not only depict the effect of aging on material stiffness and elasticity but also underscore the role of foam bitumen in mitigating aging-induced stiffness. Fig. 3c illustrates that PAV aging resulted in higher stiffness levels in CM compared to LM, particularly at higher temperatures (and/or lower frequencies). Regarding the role of fillers in foamed bitumen mastics, the most significant mitigating effect was observed with diabase fillers, while the least mitigating role was observed with basalt fillers. A similar trend is apparent in Fig. 3d, indicating the mitigating effect of foamed bitumen and filler types at higher temperatures (and/or low frequencies). This figure demonstrates that bituminous mastics produced using foamed bitumen and/or incorporating diabase fillers exhibit better resistance to gaining elasticity.

5. Micromechanical modeling

5.1. Immobilized binder layer

The micromechanical modeling approach was used to evaluate the influence of different compositions of mineral filler, to approximate the immobilized binder volume (V_{imm}) by fitting the generalized self-consistent scheme (GSCS) model. Generally, the incorporation of mineral fillers in a bituminous matrix contributes to the overall product characteristics through three main mechanisms: volume filling reinforcement, physicochemical reinforcement, and particle interaction reinforcement [28]. The stiffness of the composite matrix can be altered by each of these mechanisms, depending on whether filler concentration or interfacial contribution predominates. Notably, since the filler concentration in this study was maintained at 27 % of the total volume of the bituminous mastic, the contribution of the particle-interaction reinforcement can be disregarded.

The GSCS model, which is the interest of this section, treats the filler granules as spherical inclusions suspended in bitumen, forming a soft continuous matrix (Fig. 4). In this, the effective volumetric concentration of filler (c_{cal}) represents the volume theoretically approximated based on measured TFS results. This value can be utilized to estimate the volumetric concentration of spherical hard inclusions not associated with mineral fillers. In essence, c_{cal}, alongside the real filler concentration (c), can be used to estimate the volumetric concentration of the binder hard shell surrounding filler particles [28]. Considering the role of the actual volumetric concentration of mineral fillers in volume-filling reinforcement, the approximated binder hard shell around filler particles serves as a representative factor of physiochemical reinforcement. It is important to recall that due to the filler concentration in this research, particle reinforcement interaction can be neglected.

The volume of the hard shell surrounding the filler particles, termed V_{imm}, can be determined by subtracting c from c_{cal}, as illustrated in Eq. (4). Since the chemical composition of various filler types, combined with the aging level, influences interfacial effects between filler and bitumen, different combinations may result in distinct physicochemical reinforcement intensities. Therefore, V_{imm} serves as a representative value in this context.

$$V_{imm} = c_{cal} - c \tag{4}$$

To derive c_{cal}, the GSCS micromechanical model was applied, utilizing the TFS results of the base binder and the desired mastics as inputs, along with the shear modulus of inclusion and Poisson's ratios of inclusion and matrix. The formulation corresponding to the GSCS model is presented in Eqs. (5)–(11).

$$A\left(\frac{|G^*|_m}{|G^*|_b}\right)^2 + B\left(\frac{|G^*|_m}{|G^*|_b}\right) + C = 0 \tag{5}$$

Table 4
CAM model parameters.

Sample ID	Aging level	T_{ref} (°C)	WLF coefficients		CAM model				
			C_1	C_2	log(Gg)/[kPa]	log(ω_c)/[rad/s]	υ	m	R
CM-Unaged	Unaged	25	13.99	130.15	5.86	2.49	1.43	0.99	0.30
CM-RTFOT	RTFOT		14.51	131.74	6.09	2.16	1.65	1.01	0.30
CM-PAV	PAV		19.79	152.73	6.26	0.004	2.42	0.95	0.31
LM-Unaged	Unaged		12.74	117.70	6.11	2.49	1.59	1.04	0.29
LM -RTFOT	RTFOT		14.12	127.09	6.16	2.12	1.73	1.03	0.29
LM -PAV	PAV		12.41	93.09	6.04	0.004	2.30	1.21	0.25
BM-Unaged	Unaged		13.46	119.62	6.08	2.32	1.52	1.02	0.29
BM -RTFOT	RTFOT		14.10	128.11	6.11	2.18	1.61	1.01	0.30
BM -PAV	PAV		11.90	98.30	6.26	0.004	2.62	1.12	0.27
DM-Unaged	Unaged		14.05	128.09	5.89	2.41	1.36	0.99	0.30
DM -RTFOT	RTFOT		13.72	122.32	6.17	2.02	1.77	1.04	0.29
DM -PAV	PAV		13.54	128.55	6.64	0.004	2.64	1.28	0.23

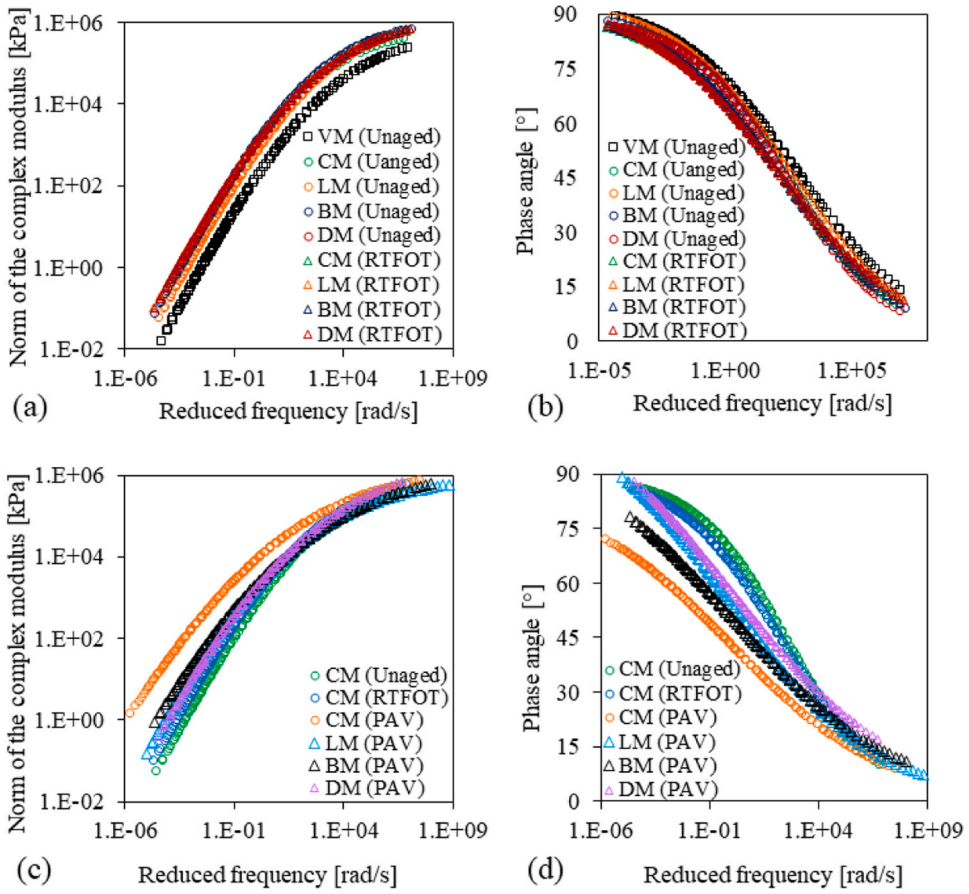

Fig. 3. Master curves of: (a, c) norm of complex modulus and (b, d) phase angle.

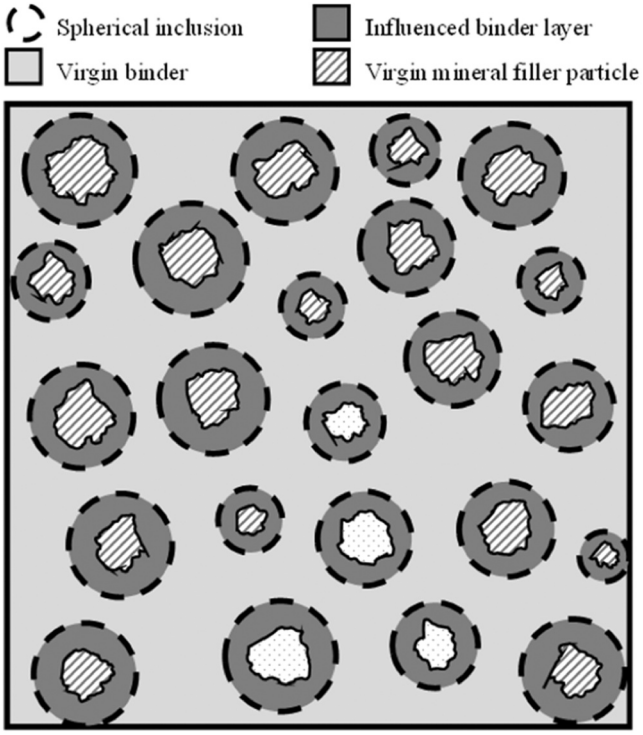

Fig. 4. Particulate composite structure of mastics based on GSCS micro-mechanical model.

$$A = 8\left(\frac{G_i}{|G^*|_b}-1\right)(4-5\nu_b)\eta_1 c^{\frac{10}{3}} - 2\left[63\left(\frac{G_i}{|G^*|_b}-1\right)\eta_2+2\eta_1\eta_3\right]c^{\frac{7}{3}} + 252\left(\frac{G_i}{|G^*|_b}-1\right)\eta_2 c^{\frac{5}{3}} - 50\left(\frac{G_i}{|G^*|_b}-1\right)(7-12\nu_b+8\nu_b^2)\eta_2 c + 4(7-10\nu_b)\eta_2\eta_3 \quad (6)$$

$$B = -4\left(\frac{G_i}{|G^*|_b}-1\right)(1-5\nu_b)\eta_1 c^{\frac{10}{3}} + 4\left[63\left(\frac{G_i}{|G^*|_b}-1\right)\eta_2+2\eta_1\eta_3\right]c^{\frac{7}{3}} - 504\left[\left(\frac{G_i}{|G^*|_b}-1\right)\eta_2\right]c^{\frac{5}{3}} + 150\left(\frac{G_i}{|G^*|_b}-1\right)(3-\nu_b)\nu_b\eta_2 c + 3(15\nu_b-7)\eta_2\eta_3 \quad (7)$$

$$C = 4\left(\frac{G_i}{|G^*|_b}-1\right)(5\nu_b-7)\eta_1 c^{\frac{10}{3}} - 2\left[63\left(\frac{G_i}{|G^*|_b}-1\right)\eta_2+2\eta_1\eta_3\right]c^{\frac{7}{3}} + 252\left(\frac{G_i}{|G^*|_b}-1\right)\eta_2 c^{\frac{5}{3}} + 25\left(\frac{G_i}{|G^*|_b}-1\right)(\nu_b^2-7)\eta_2 c - (7+5\nu_b)\eta_2\eta_3 \quad (8)$$

$$\eta_1 = \left(\frac{G_i}{|G^*|_b}-1\right)(49-50\nu_i\nu_b) + 35\frac{G_i}{|G^*|_b}(\nu_i-2\nu_b) + 35 \quad (2\nu_i-\nu_b) \quad (9)$$

$$\eta_2 = 5\nu_i\left(\frac{G_i}{|G^*|_b}-8\right) + 7\left(\frac{G_i}{|G^*|_b}+4\right) \quad (10)$$

$$\eta_3 = \frac{G_i}{|G^*|_b} \quad (8 - 10\nu_b) + (7 - 5\nu_b) \tag{11}$$

where $|G^*|_m$ and $|G^*|_b$ are the norm of the complex modulus of the mastic and base binder, respectively, acquired through the TFS testing; G_i is the shear modulus of the inclusion (i.e. mineral fillers); υ_b and υ_i are the Poisson's ratios corresponding to the base binder and inclusion, respectively. G_i, υ_b, and υ_i were set to 24 GPa, 0.4, and 0.15, respectively, aligning with the assumptions made in previous research studies.

Relying on the relationships in Eqs. (5)–(11), the value of c is iteratively back-calculated by minimizing the convergence error between the measure and predicted $|G^*|_m$ values, thereby determining c_{cal}. To highlight the combined influence of temperature and aging on the influenced binder layer, TFS results were solely utilized at the reference angular frequency of 10 rad/s across the tested temperatures to back-calculate c_{cal} and subsequently the V_{imm}. Fig. 5 summarizes the results of GSCS micromechanical model, representing V_{imm} of the mastics at various aging levels across a temperature range.

In this figure, the phenomenon of physicochemical-induced stiffening (associated with interfacial interaction of filler and binder) can be assessed, where V_{imm} values associated with unaged mastics varied in the range of 0.16–0.38. Given the volumetric concentration of mineral fillers set at 27 %, it can be inferred that interfacial stiffening deviated from the filler type.

Further, the impact of temperature is evident, demonstrating a gradual increase in V_{imm} with rising temperature up to intermediate conditions, while V_{imm} values remained almost constant in high-temperature conditions. Comparing various aging levels underscores the significant role of aging protocols in forming higher volumes of immobilized binder. Exposure to the PAV aging protocol notably increased the volume of immobilized binder, surpassing even the values associated with unaged and RTFOT-aged mastics. Similar to V_{imm} curves of unaged bituminous mastics, increasing the temperature from low to intermediate levels increased the volume of immobilized binder, while at temperatures above the intermediate range, the component reached a steady state. While this observation suggests that aging intensity plays a more significant role in shaping the immobilized binder layer compared to other considered factors, it can be inferred that the role of various filler components in mitigating aging-induced stiffening becomes more apparent at higher levels of aging.

5.2. Thickness of adsorbed binder layer

Given that the mineral fillers' concentration remained consistent across all variants, any rheological and chemical differences among different bituminous mastics can be attributed to the physicochemical reinforcement resulting from the interfacial interaction between the inclusion and matrix. Among the micromechanical models, the Hashin model is an analytical tool to assess the impact of physicochemical interaction alongside filler-filling reinforcement [25].

The Hashin model is primarily designed for analyzing an isotropic heterogeneous medium containing spherical-shaped inclusions. Within this framework, the effective shear modulus of the desired composite, which constitutes a two-phase linear elastic composite, can be determined using the following relationship in Eq. (12).

$$\frac{G_c}{G_m} = 1 + \frac{15(1-\nu_m)\left(\frac{G_f}{G_m} - 1\right)\varphi_f}{7 - 5\nu_m + 2(4-5\nu_m)\left[\frac{G_f}{G_m} - \left(\frac{G_f}{G_m} - 1\right)\varphi_f\right]} \tag{12}$$

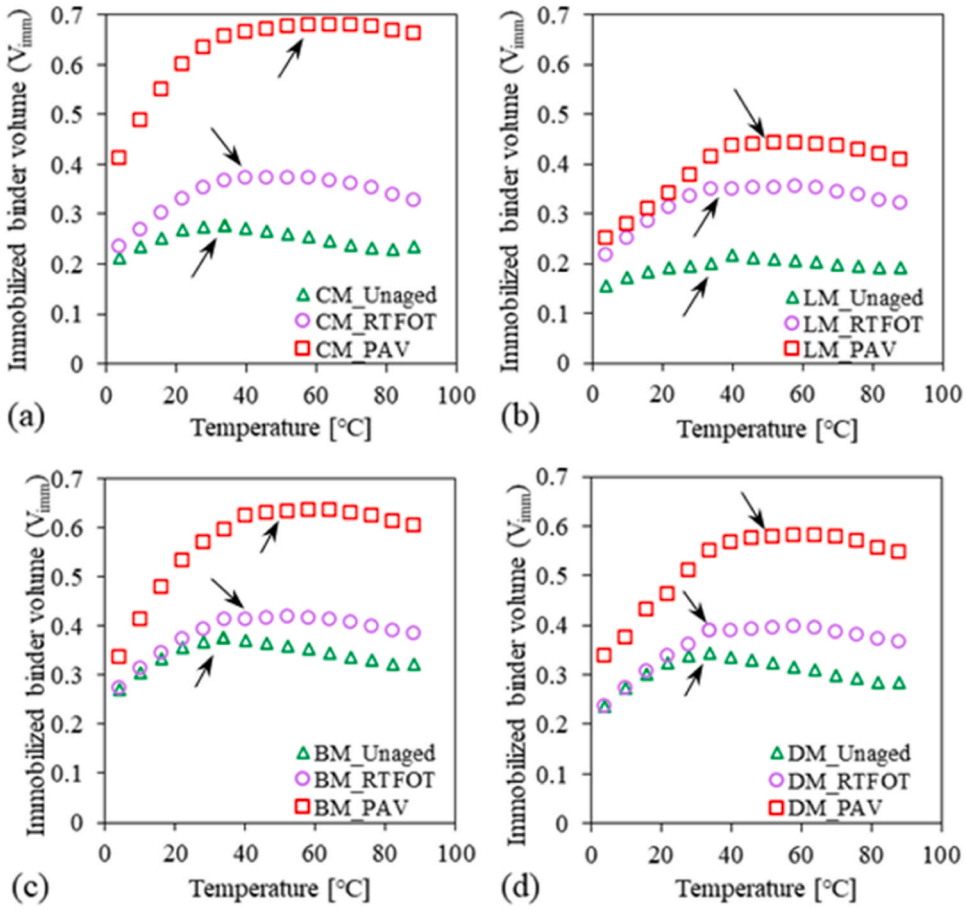

Fig. 5. Immobilized binder volume of various mastics; a) control mastics, b) limestone mastics, c) basalt mastics, and d) diabase mastics.

where G_c is the effective shear modulus of composite mastic; G_m is the shear modulus of matrix; G_f is the shear modulus of filler; υ_m is the Poisson's ratio of matrix; and φ_f is the volume fraction of filler. In the context of bituminous mastics, the abovementioned model can be simplified by assuming that G_f is significantly greater than G_m. Therefore, the relationship presented in Eq. (13) can be restructured as shown in Eq. (13).

$$\frac{G_c}{G_m} = 1 + \frac{15(1-\nu_m)\varphi_f}{2(4-5\nu_m)(1-\varphi_f)} \tag{13}$$

Given that the model presented in Eq. (13) only considers the reinforcement causes by the volume-filling phenomenon, the role of physicochemical interactions between the mineral filler and the asphalt binder can be incorporated into the computation by replacing φ_f with φ_{ff}. The former is the actual filler concentration in the mastic while the latter is the effective volume fraction of mineral filler. Thereafter, the total volume of the adsorbed binder together with the volume of filler inclusion can be achieved by back-calculating the value of φ_{ff}. Having in hand the values of φ_f, φ_{ff}, and physical characteristics of mineral filler, the thickness of adsorbed binder layer can be calculated through Eqs. (14) and (15).

$$\varphi_{eff} = \frac{2\left(\frac{G_c}{G_m}-1\right)(4-5\nu_m)}{15(1-\nu_m)+2\left(\frac{G_c}{G_m}-1\right)(4-5\nu_m)} \tag{14}$$

$$d = \frac{\varphi_{eff}-\varphi_f}{\varphi_f \times g \times s} \tag{15}$$

where d is the film thickness (μm); g is specific weight of filler (g/μm^3); s is specific surface area of the filler (μm^2/g).

To determine the thickness of the adsorbed binder film in this study, the master curves developed by the CAM model were employed as the input values, determining the simultaneous impacts of temperature and frequency on shaping distinct thicknesses of adsorbed binder layers. It has been noted in the literature that higher temperatures lead to increased thicknesses of the adsorbed binder layer [28], while thickness decreases as frequency increases [25]. Fig. 6 depicts the approximated values of the adsorbed binder thickness, indicating that aging protocols resulted in increased thicknesses of the adsorbed binder layer. Besides the governing role of aging, both temperature and frequency played significant roles in shaping this component. The influence of mineral filler components on the thickness of the layer is also apparent, emphasizing the physicochemical-induced stiffness in bituminous mastics.

Fig. 6 depicted that increased angular frequencies decrease the thickness of the adsorbed binder layer, and similarly, higher temperatures, associated with lower reduced frequencies, result in greater binder thicknesses. These two observations were aligned with the findings of previous research works. However, beyond intermediate temperatures (i.e. 28–34 °C), the thickness of the adsorbed binder layer reaches a local limit, suggesting a limitation in forming the adsorbed binder layer despite the exposure to high temperatures. This value varies depending on the mineral composition of the filler and aging intensity, implying the role of different fillers' mineral compositions in absorbing the polar components of asphalt binder.

From the perspective of filler mineral composition, the results of the adsorbed film thickness can be analyzed in relation to the origin of different fillers. The role of mineral filler composition can be investigated in different manners, where these components solely lead to distinct film thicknesses in unaged mastics. Further, their contribution to aging protocols and the mixture technology in shaping distinctive film thicknesses is of interest to the field. Firstly, mastics incorporating

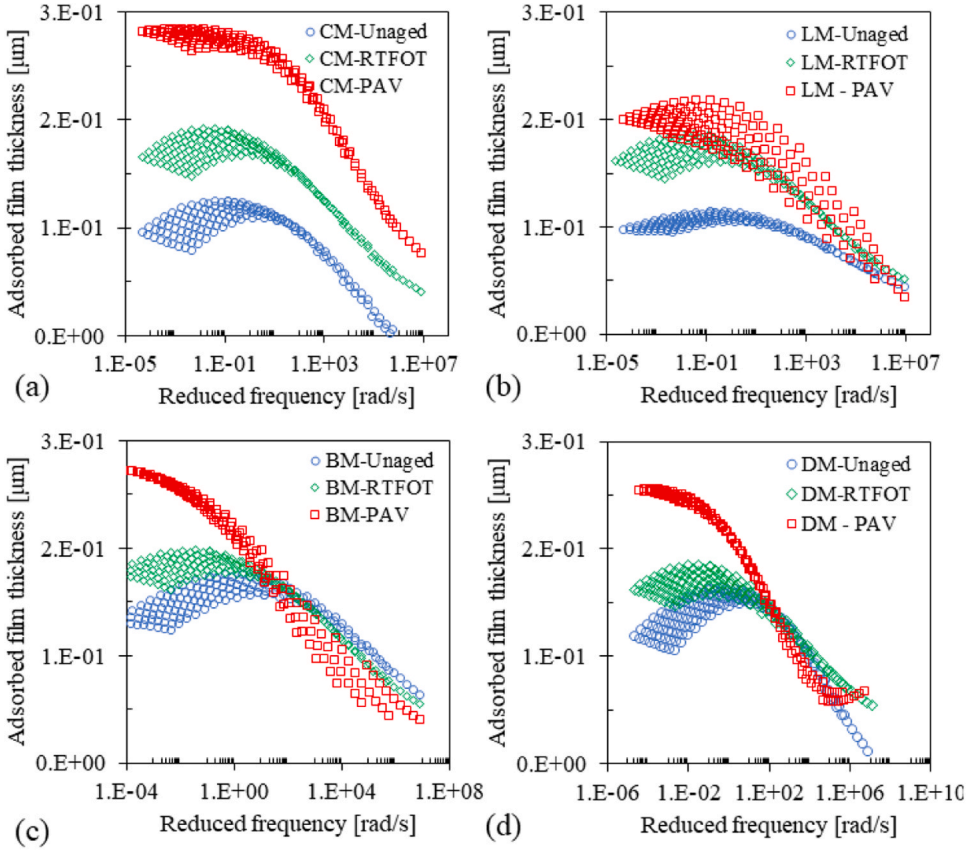

Fig. 6. Adsorbed film thickness variation of various mastics; a) control mastics, b) limestone mastics, c) basalt mastics, and d) diabase mastics.

limestone fillers (produced using water-based foamed bitumen) exhibit thinner film thicknesses compared to those incorporating basalt and diabase fillers. Additionally, a notable decrease in the thickness of the adsorbed film is apparent with the use of foaming technology when comparing the CM and LM.

Fig. 6b illustrates that PAV-aged LM mastics exhibit a high degree of dependency on the combination of temperatures and angular frequencies. This indicates that the use of foamed bitumen and the incorporation of limestone fillers render the film thicknesses sensitive to changes in angular frequencies. In contrast, a comparison of the plots in Fig. 6b–d revealed that the inclusion of basalt and diabase significantly reduces the dependency of film thicknesses on temperature changes. To elaborate further, the film thickness curve associated with PAV-aged diabase mastics follows a continuous shape without any disruptions across various combinations of temperature/frequency. This suggests that when mastics incorporate diabase fillers, the impact of angular frequencies on film thickness at specific temperatures is lower compared to mixes incorporating limestone and basalt.

5.3. Discussion on the adsorbed/immobilized binder fractions

The micromechanical modeling results unveiled that the combination of aging levels and the fillers composition influenced the relationship between temperature and immobilized binder volumes. As depicted in Fig. 5, increasing the temperature led to higher immobilized binder volumes until reaching a steady equilibrium point, indicated by arrows. Notably, aged mastics necessitated higher temperatures to reach this equilibrium point. This observation underscores the significance of binder viscosity in the formation of the immobilized binder fraction, as it enables bitumen to sufficiently cover the fillers and facilitates the attraction of polar components in bitumen to the surface of mineral fillers. However, at temperatures exceeding that corresponding to this equilibrium point, the role of temperature becomes less significant as the bitumen has already transitioned to its required liquid state. Fig. 7 illustrates the role of temperature on the formation of the immobilized binder fraction.

Besides, the adsorbed binder thicknesses signified the concurrent impact of temperature and frequency. At lower reduced frequencies, corresponding to higher temperatures, angular frequency played a crucial role in forming the adsorbed binder layer, while its impact was opposite at conditions associated with higher reduced frequencies. Additionally, heightened aging levels, attributable to increased viscosity, diminished the importance of angular frequency. These findings underscore the role of mixture viscosity in shaping the adsorbed binder layer, while angular frequency predominates in scenarios where the mixture exhibits lower viscosity.

6. Chemical characteristics

To assess the aging intensity across different bituminous mastics, FTIR spectroscopy results underwent preprocessing according to [40], followed by calculating indices for carbonyl (1725–1665 cm^{-1}) and sulfoxide (1070–984 cm^{-1}) functional groups by integrating areas beneath normalized spectral curves. Fig. 8 illustrates the distribution of these indices, revealing an increase in the carbonyl index due to PAV aging compared to the mastics with RTFOT. On the other hand, at the post-PAV aging stage, the mastics containing diabase fillers exhibited higher carbonyl levels compared to other filler types. Moreover, within the realm of bitumen technology, the carbonyl index in CM (limestone fillers and base binder) was significantly lower than in LM (limestone and foamed bitumen).

Regarding sulfoxide indices, BM and DM variants, both unaged and RTFOT-aged, demonstrated notably higher values compared to mastics with limestone fillers. Conversely, PAV aging led to a significant increase in the sulfoxide index for CM, surpassing even LM values. This observation suggests that the higher sulfoxide levels in unaged and RTFOT-aged BM and DM mastics may be attributed to the mineral filler compositions, while the relatively lower index of PAV-aged LM and DM compared to CM can be inferred as the role of foam bitumen in mitigating the aging-induced chemical changes.

To wrap up this part, contrasting phenomena were observed in various aging indices, where the role of foam bitumen was catalyzing the formation of carbonyl while mitigating sulfoxide increase. Assuming the carbonyl and sulfoxide functional groups are representative of aging levels, interpreting the role of mineral components alongside bitumen technology on aging evolution is challenging. To address this, the contribution of chemical components to rheological and micromechanical characteristics will be discussed further.

The evolution of carbonyl and sulfoxide functional groups was investigated in conjunction with rheological parameters, specifically the cross-over frequency (ω_c), as shown in Fig. 9. This figure reveals a noticeable consistency among points corresponding to a similar aging level. Notably, an increase in aging level correlated with a decrease in the value of ω_c across the examined bituminous mastics, consistent with findings in the literature [41]. Furthermore, Fig. 9 highlights the intensity of the respective indices relative to the mineral composition of the fillers used, at each aging level. This comparison offers insights into both the chemical and rheological characteristics of the mastics.

7. Chemo-mechanical characteristics of bituminous mastics

Investigating the chemical, rheological, and micromechanical characteristics of bituminous mastics has yielded distinctive information related to various domains of bituminous mastics characteristics. Understanding these characteristics necessitates an analysis of their interactions and simultaneous contributions. Hence, the clustering approach, a form of an unsupervised learning algorithm in the realm of machine learning (ML) [42], was selected to categorize the dataset into distinct clusters.

Initially, the dataset comprising chemical indices values was analyzed using a clustering approach to classify it into subsets representing different aging states in bituminous mastics. The mastics were plotted in a 2D graph based on carbonyl and sulfoxide values, though these results are not presented here due to brevity. This analysis showed that it is difficult to distinguish various clusters from the examined mastics based on those chemical compositions. Subsequently, a dataset comprising (i) chemical indices, (ii) immobilized binder volumes (section 5–1), and (iii) adsorbed binder thicknesses (section 5–2) was prepared. Given the complexity of the dataset, the Principal Component Analysis (PCA), an unsupervised learning algorithm, was employed to project the dataset into a new space with comparable representation levels. Hierarchical Cluster Analysis (HCA) was then utilized to identify various clusters. Both PCA and HCA are multivariate data analysis techniques capable of yielding reasonable groupings.

Python programming language was utilized for the analysis, employing *PCA* and *AgglomerativeClustering* analyses from the *sklearn*

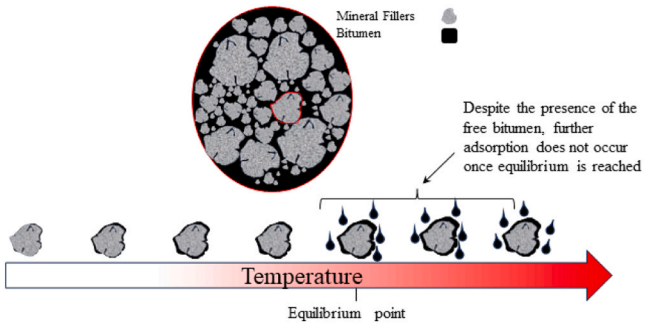

Fig. 7. Representing the role of temperature in forming the immobilized binder layer.

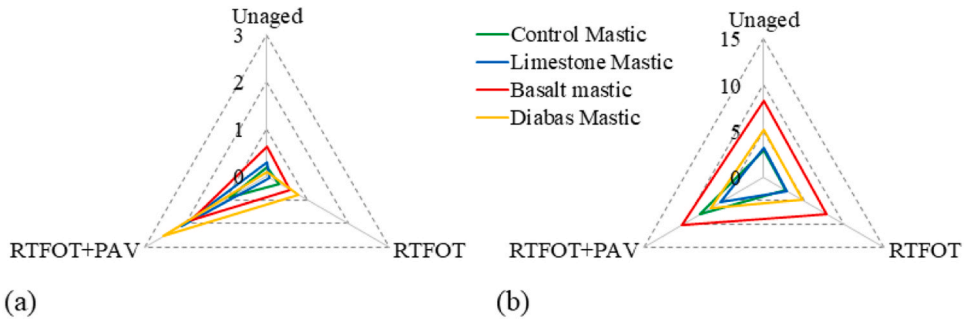

Fig. 8. Distribution of function groups in the bituminous mastics at various aging levels; (a) carbonyl and (b) sulfoxide functional groups.

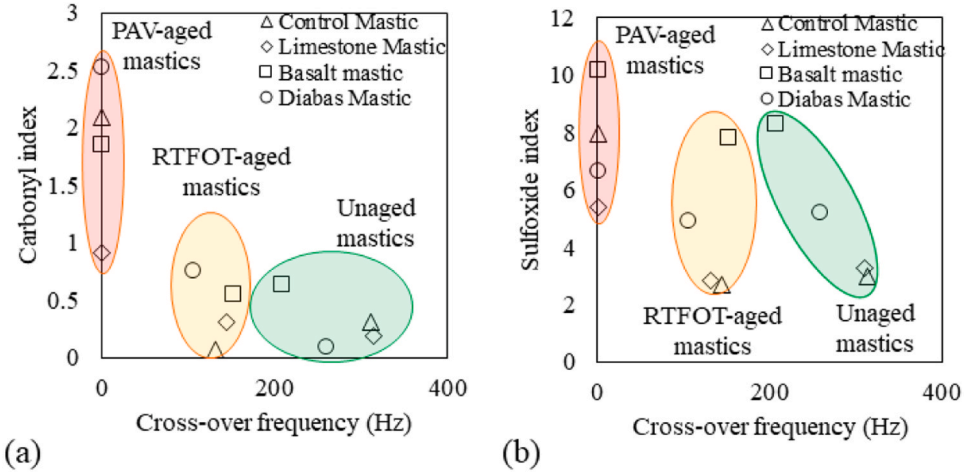

Fig. 9. Carbonyl (a) and sulfoxide (b) functional groups indices against the cross-over frequency.

library. The analysis commenced with determining the explained variance ratios of multiple principal components in PCA, as shown in Fig. 10a. It was revealed that three principal components are necessary to adequately explain the phenomena using PCA analysis. Three components resulted in a new dataset representation shown in Fig. 10b–d. While PC1 was identified as the most representative component for distinguishing aging levels, it was challenging to establish a clear decision boundary between unaged and RTFOT-aged mastics on PC1 values alone. However, focusing on PC3 elucidated these values are slightly greater than those of unaged mastics, suggesting potential utility in distinguishing between mastics in a 3D projection.

Integrating PCA results into HCA analysis led to the division of the data surface into four distinct clusters as per Fig. 11a. This clustering was attributed to the interaction between filler mineral composition and aging protocols, termed physicochemical interactions. For instance, cluster 1 comprised LM and CM mastics before and after RTFOT, while cluster 2 included all BM mastics (i.e., unaged, RTFOT, and PAV) and PAV-aged CM variant. Comparison between these revealed similarities in physicochemical characteristics of PAV-aged CM mastic and BM mastic variants, suggesting a relationship between aging protocols and mastic compositions. In the same way, unaged and RTFOT-aged CM mastic variants were included in the same cluster (cluster 1) with unaged and RTFOT-aged LM variants. Cluster 4 encompassed PAV-aged LM and DM variants, while Cluster 3 represented unaged and RTFOT-aged DM mastics.

To enhance the differentiation further, an alternative dimensionality reduction technique, Partial Least-Squares Regression (PLSR), was employed. Unlike PCA, PLSR is a supervised learning approach that considers data labels during dimensionality reduction. To facilitate this, the label matrix was encoded for compatibility with regression-based algorithms. Subsequently, the latent variables (LVs) underlying the input dataset were determined by fitting a PLSR model. The distribution of LV importance, shown in Fig. 12a-b, revealed that six latent variables were necessary to adequately explain the variance between samples in the dataset, with no significant improvement observed beyond this point. Notably, the primary variance could be reasonably explained by the first two LVs. (Fig. 12b).

Upon fitting the PLSR model with six LVs, the corresponding weights for each variable were determined as displayed in Fig. 12c and d. Subsequently, a new data set comprising two label features (mastic type and aging level) along with the six LVs was generated. Clustering analysis was then conducted using the HCA algorithm, defining four clusters. The results depicted in Fig. 13 revealed distinct clusters, with PAV-aged CM forming its own cluster (cluster 4). Additionally, PAV-aged BM and DM mastics were grouped together in cluster 2, while cluster 3 encompassed unaged variants of CM and LM. Cluster 1 comprised all RTFOT-aged variants, along with PAV-aged LM and unaged variants of DM and BM.

The results of the clustering task revealed that the point representing PAV-aged LM appears relatively close to cluster 2, where the physicochemical characteristics of PAV-aged DM and BM are evident. This suggests that while the characteristics of PAV-aged LM are well represented by cluster 1, the trace of PAV-aged (foamed) WMA mastics is apparent. Similarly, the points representing unaged DM and BM variants are projected in the lower left part of cluster 2, likely due to their contrasting properties compared to PAV-aged LM (and in PAV-aged WMA mastics). All the RTFOT-aged variants are centrally located within cluster 1, with reasonable overlap.

Examining the clustering pattern in Fig. 13, it's apparent that points corresponding to various aging states are projected closely together, while differences in mineral components (filler types) and mix technology (foamed or base bitumen) dictate the formation of distinct clusters. This observation underscores the robustness of the

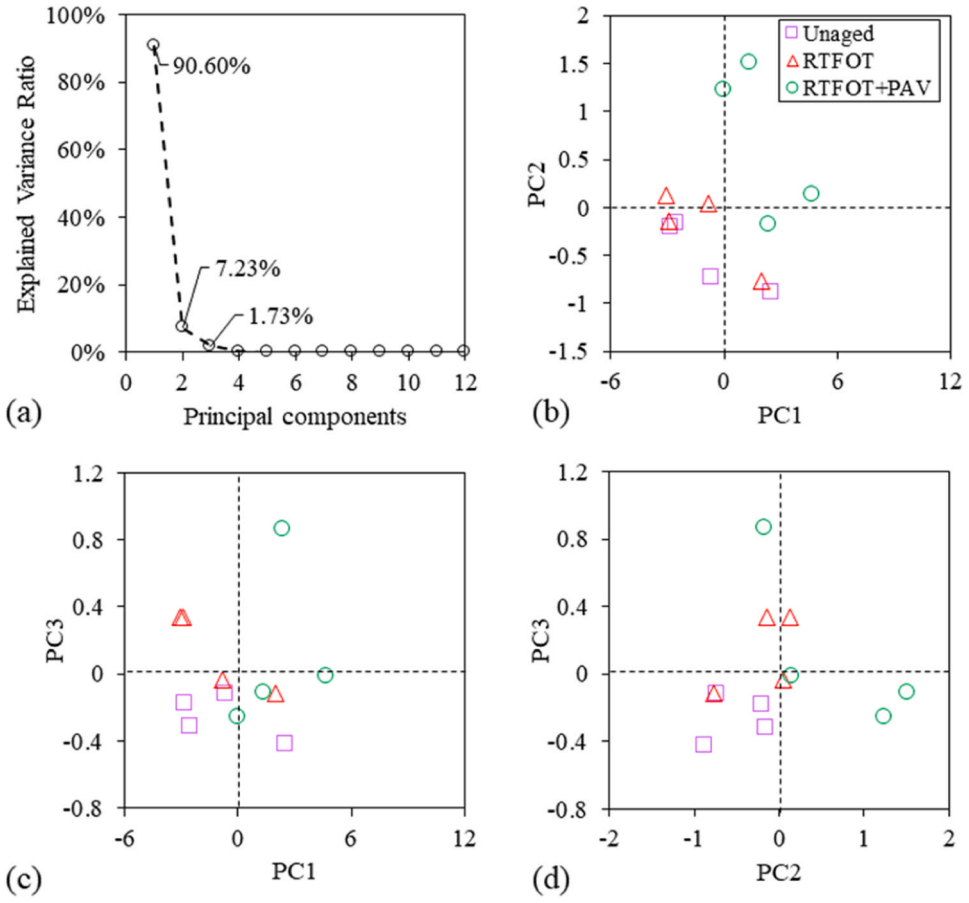

Fig. 10. PCA multivariate analysis criteria; (a) the importance of principal components, (b-d) binary projection of PCs.

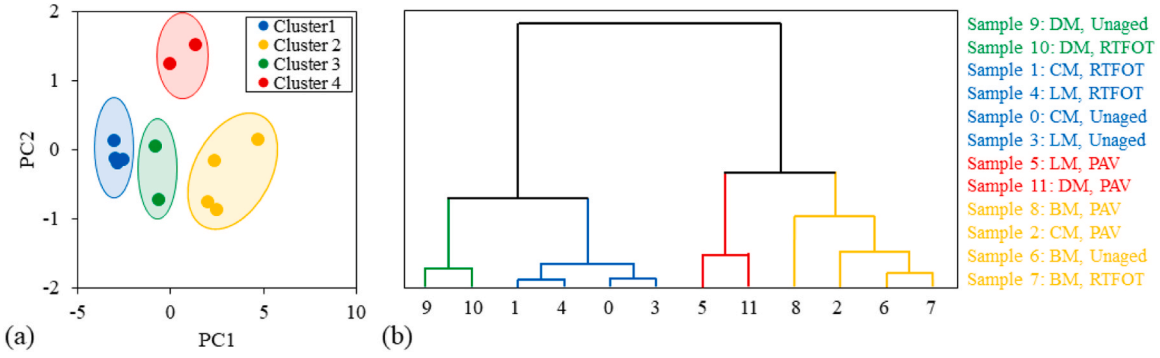

Fig. 11. Results of clustering task using PCA-HCA; (a) clusters boundary, (b) Hierarchical clustering dendrogram.

simultaneous use of PLSR and HCA, referred to as PLSR-HCA, in analyzing datasets comprising indies from FTIR results and micromechanical modeling results. Consequently, it can be concluded that different bituminous mastics can be effectively distinguished into various clusters by analyzing their chemical characteristics and attributes related to binder adsorption using the PLSR-HCA clustering approach.

8. Conclusions

The present research was drawn aiming at characterizing the physicochemical interactions between the mineral components and bituminous binder induced by aging phenomenon in the bituminous mastics. To discover this phenomenon various bituminous mastics with various aging levels were exposed to TFS and FTIR testing, resulting in time-temperature-dependent responses and chemical characteristics of the produced product. The TFS results were initially analyzed by implementing a CAM modeling approach to fit the master curves and determine the inputs of micromechanical modeling. On one side, two well-known micromechanical modeling approaches, termed as GSCS and Hashin model, were employed to characterize the immobilized binder volume and adsorbed binder thicknesses, respectively. On the other hand, the FTIR results were employed to calculate the indices representing the aging-related functional groups. Combining these three sources of data, the role of the aging process in altering the physicochemical interaction between the constituted components can be explained. To do so, a clustering approach relying on the ML algorithms was employed to unveil the latent relationship between the variables by

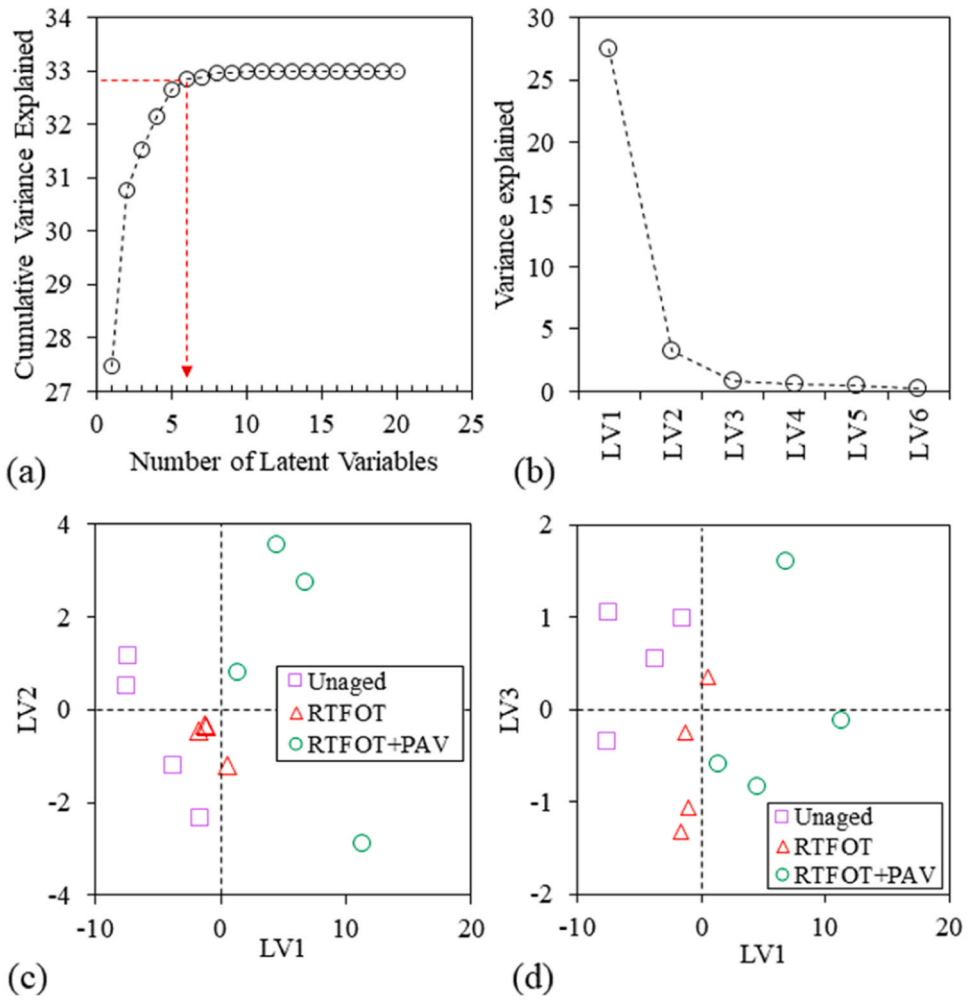

Fig. 12. PLSR multivariate criteria: (a) cumulative variance explained, (b) the exact variance explained by each LV, (c-d) separation of various samples based on LVs.

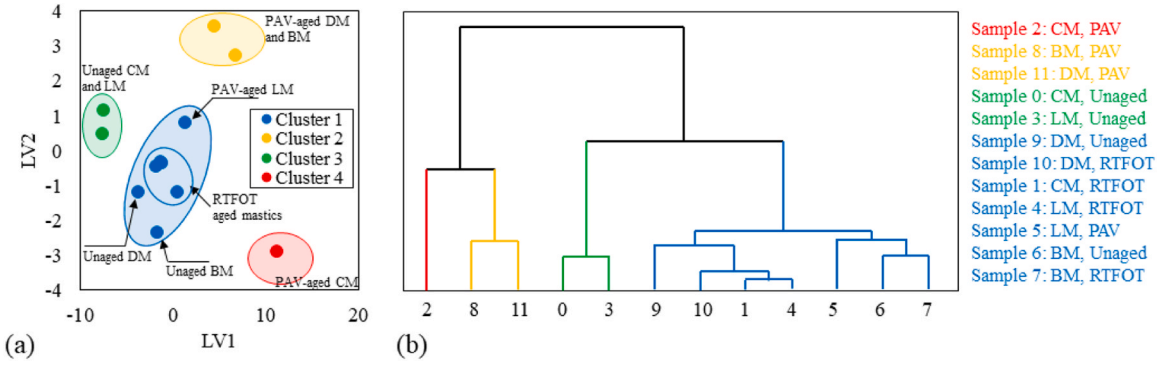

Fig. 13. Results of clustering task using PLSR-HCA; (a) clusters boundary, (b) Hierarchical clustering dendrogram.

discovering the clusters within the dataset. This methodology resulted in findings as follows:

1) The application of aging protocols on bituminous mastics led to a gradual alteration in their rheological properties, resulting in increased stiffness with higher levels of aging. This trend was evident in the cross-over frequency values, which decreased with higher aging levels.
2) The influence of aging accumulation on the rheological properties of bituminous mastics varied depending on the type of mineral fillers used. Diabase filler demonstrated a mitigating effect when combined with foamed bitumen technology, reducing aging-induced stiffness, whereas basalt fillers contributed to the highest stiffness levels among the tested mixes.
3) Throughout rheological analyses, the impact of aging protocols, mineral fillers, and bitumen technology on the physicochemical interactions in bituminous mastics was apparent. The GSCS micromechanical model was utilized to evaluate the volume of immobilized binder, reflecting these interactions. Results showed a significant increase in immobilized binder volume due to aging accumulation, catalyzing physicochemical interactions.

4) The Hashin model was employed to estimate the thickness of adsorbed binder in various bituminous mastics, reflecting changes in physicochemical interactions. Consistent with the GSCS model, the Hashin model results confirmed the role of aging in increasing the thickness of the adsorbed binder layer. The role of temperature was also in the same term, where higher temperatures increased thicknesses. On the role of mineral fillers, the incorporation of diabase filler led to a more consistent evolution of adsorbed binder thicknesses compared to limestone fillers. This model highlighted the foamed bitumen technology influencing this phenomenon.
5) Chemical composition analysis of bituminous mastics revealed insights into carbonyl and sulfoxide functional groups. These indices highlighted the impact of mineral fillers and bitumen technologies on forming desired functional groups. Diabase fillers catalyzed the formation of carbonyl groups, while basalt fillers played a similar role in forming sulfoxide functional groups.
6) Chemo-mechanical analysis using PLSR-HCA clustering revealed four distinct clusters based on interactions between mineral components, bitumen characteristics, and aging levels. This clustering emphasized the significant roles of aging and mineral composition in shaping physicochemical interactions. Considering both chemical and mechanical characteristics in PLSR-HCA clustering, limestone fillers in foamed bitumen technology appeared to mitigate aging-induced stiffness in mastics. This observation was supported by the assignment of PAV-aged LM to cluster 1, indicating lower aging intensities.
7) The research findings indicate that the integration of ML algorithms with experimental investigations can significantly enhance the design specifications of asphalt mixtures. This approach addresses the issue of aging in asphalt over its lifespan. Such integration is particularly beneficial for the asphalt industry, especially in the context of high-RAP mixtures, which incorporate more than 25 % RAP. Additionally, the role of various mineral fillers in the aging evolution of recycled asphalt mixtures presents a promising area for future research.

CRediT authorship contribution statement

Seyed Mohsen Motevalizadeh: Writing – original draft, Software, Methodology, Investigation, Formal analysis, Data curation, Conceptualization. **Konrad Mollenhauer:** Writing – review & editing, Supervision, Project administration, Methodology, Conceptualization.

Declaration of Competing Interest

The authors declare that they have no known competing financial interests or personal relationships that could have appeared to influence the work reported in this paper.

Data availability

Data will be made available on request.

References

[1] F. Mastoras, A. Varveri, M. van Tooren, S. Erkens, Effect of mineral fillers on ageing of bituminous mastics, Constr. Build. Mater. 276 (2021), https://doi.org/10.1016/j.conbuildmat.2020.122215.
[2] C. Davis, C. Castorena, Implications of physico-chemical interactions in asphalt mastics on asphalt microstructure, Constr. Build. Mater. 94 (2015) 83–89, https://doi.org/10.1016/j.conbuildmat.2015.06.026.
[3] Y. Zhang, T. Ma, M. Ling, D. Zhang, X. Huang, Predicting dynamic shear modulus of asphalt mastics using discretized-element simulation and reinforcement mechanisms, J. Mater. Civ. Eng. 31 (2019), https://doi.org/10.1061/(asce)mt.1943-5533.0002831.
[4] X. Zhu, Z. Du, H. Ling, L. Chen, Y. Wang, Effect of filler on thermodynamic and mechanical behaviour of asphalt mastic: a MD simulation study, Int. J. Pavement Eng. 21 (2020) 1248–1262, https://doi.org/10.1080/10298436.2018.1535120.
[5] R. Moraes, H.U. Bahia, Effect of mineral filler on changes in molecular size distribution of asphalts during oxidative aging, Asph. Paving Technol. Assoc. Asph. Paving Technol. Tech. Sess. 84 (2015) 79–114, https://doi.org/10.1080/14680629.2015.1076998.
[6] T.W. Kennedy, R.J. Cominsky, E.T. Harrigan, R.B. Leahy, Hypotheses and Models Employed in the SHRP Asphalt Research Program, 1990.
[7] F. Li, Y. Yang, L. Wang, The interfacial interaction between asphalt binder and mineral filler: a comprehensive review on mechanisms, evaluation methods and influence factors, Int. J. Pavement Eng. 23 (2022) 4291–4305, https://doi.org/10.1080/10298436.2021.1942468.
[8] J. Pei, Z. Fan, P. Wang, J. Zhang, B. Xue, R. Li, Micromechanics prediction of effective modulus for asphalt mastic considering inter-particle interaction, Constr. Build. Mater. 101 (2015) 209–216, https://doi.org/10.1016/j.conbuildmat.2015.10.053.
[9] J. Zhang, G. Liu, C. Zhu, J. Pei, Evaluation indices of asphalt–filler interaction ability and the filler critical volume fraction based on the complex modulus, Road. Mater. Pavement Des. 18 (2017) 1338–1352, https://doi.org/10.1080/14680629.2016.1218789.
[10] J. Wang, T. Wang, X. Hou, F. Xiao, Modelling of rheological and chemical properties of asphalt binder considering SARA fraction, Fuel 238 (2019) 320–330, https://doi.org/10.1016/j.fuel.2018.10.126.
[11] M. Guo, A. Bhasin, Y. Tan, Effect of mineral fillers adsorption on rheological and chemical properties of asphalt binder, Constr. Build. Mater. 141 (2017) 152–159, https://doi.org/10.1016/j.conbuildmat.2017.02.051.
[12] A. Kavussi, S.M. Motevalizadeh, Fracture and mechanical properties of water-based foam warm mix asphalt containing reclaimed asphalt pavement, Constr. Build. Mater. (2020) 121332, https://doi.org/10.1016/j.conbuildmat.2020.121332.
[13] M. Ameri, M.H. Mohammadi, S.M. Motevalizadeh, A. Mousavi, Experimental study to investigate the performance of cold in-place recycling asphalt mixes, Proc. Inst. Civ. Eng. Transp. 172 (2019) 360–370, https://doi.org/10.1680/jtran.17.00062.
[14] S. Mohsen Motevalizadeh, A. Kavussi, K. Mollenhauer, C. Vuye, N. Hasheminejad, Use of a machine learning-based framework to approximate the input features of an intrinsic cohesive zone model of recycled asphalt mixes tested at low temperatures, Constr. Build. Mater. 373 (2023), https://doi.org/10.1016/j.conbuildmat.2023.130870.
[15] D.E. Newcomb, E. Arambula, F. Yin, J. Zhang, A. Bhasin, W. Li, Z. Arega, Prop. Foam. Asph. Warm Mix Asph. Appl, Prop. Foam. Asph. Warm. Mix Asph. Appl. (2015), https://doi.org/10.17226/22145.
[16] B.K. Bairgi, U.A. Mannan, R.A. Tarefder, Tribological evaluation for an in-depth understanding of improved workability of foamed asphalt, Transp. Res. Rec. 2673 (2019) 533–545, https://doi.org/10.1177/0361198119835510.
[17] B. Huang, Y. Zhang, X. Shu, Y. Liu, D. Penumadu, X.P. Ye, Neutron scattering for moisture detection in foamed asphalt, J. Mater. Civ. Eng. 25 (2013) 932–938, https://doi.org/10.1061/(asce)mt.1943-5533.0000762.
[18] B.K. Bairgi, R.A. Tarefder, Effect of foaming water contents on high-temperature rheological characteristics of foamed asphalt binder, Int. Conf. Transp. Dev. 2018 Airf. Highw. Pavements - Sel. Pap. from Int. Conf. Transp. Dev. 2018 (2018) 243–251, https://doi.org/10.1061/9780784481554.025.
[19] B.K. Bairgi, U.A. Mannan, R.A. Tarefder, Influence of foaming on tribological and rheological characteristics of foamed asphalt, Constr. Build. Mater. 205 (2019) 186–195, https://doi.org/10.1016/j.conbuildmat.2019.02.009.
[20] K. Maciejewski, A. Chomicz-Kowalska, E. Remisova, Effects of water-foaming and liquid warm mix additive on the properties and chemical composition of asphalt binders in terms of short term ageing process, Constr. Build. Mater. 341 (2022) 127756, https://doi.org/10.1016/j.conbuildmat.2022.127756.
[21] A.M. Hung, A. Goodwin, E.H. Fini, Effects of water exposure on bitumen surface microstructure, Constr. Build. Mater. 135 (2017) 682–688, https://doi.org/10.1016/j.conbuildmat.2017.01.002.
[22] B.S. Underwood, Y.R. Kim, A four phase micro-mechanical model for asphalt mastic modulus, Mech. Mater. 75 (2014) 13–33, https://doi.org/10.1016/j.mechmat.2014.04.001.
[23] W.G. Buttlar, D. Bozkurt, G.G. Al-Khateeb, A.S. Waldhoff, Understanding asphalt mastic behavior through micromechanics, Transp. Res. Rec. (1999) 157–169, https://doi.org/10.3141/1681-19.
[24] Z. Hashin, S. Shtrikman, A variational approach to the theory of the elastic behaviour of multiphase materials, J. Mech. Phys. Solids 11 (1963) 127–140, https://doi.org/10.1016/0022-5096(63)90060-7.
[25] F. Li, Y. Yang, L. Wang, Evaluation of physicochemical interaction between asphalt binder and mineral filler through interfacial adsorbed film thickness, Constr. Build. Mater. 252 (2020), https://doi.org/10.1016/j.conbuildmat.2020.119135.
[26] E. Herve, A. Zaoui, n-Layered inclusion-based micromechanical modelling, Int. J. Eng. Sci. 31 (1993) 1–10, https://doi.org/10.1016/0020-7225(93)90059-4.
[27] R.M. Christensen, K.H. Lo, Solutions for effective shear properties in three phase sphere and cylinder models, J. Mech. Phys. Solids 27 (1979) 315–330, https://doi.org/10.1016/0022-5096(79)90032-2.
[28] S.M. Motevalizadeh, A. Kavussi, L. Tsantilis, D. Dalmazzo, E. Santagata, Investigating the influence of fine RAP on bituminous mixtures at the mastic scale: viscoelastic analyses and micromechanical modelling, Int. J. Pavement Eng. (2021) 1–11, https://doi.org/10.1080/10298436.2021.2017433.
[29] L.D. Poulikakos, B. Hofko, A. Cannone Falchetto, L. Porot, G. Ferrotti, J. Grenfell, Recommendations of RILEM TC 252-CMB: relationship between laboratory short-term aging and performance of asphalt binder, Mater. Struct. Constr. 52 (2019), https://doi.org/10.1617/s11527-019-1370-9.
[30] A. Kavussi, S.M. Motevalizadeh, Fracture failure evaluation of foam WMA Mixes containing RAP by applying weibull probability distribution function, Int. J. Pavement Res. Technol. (2021), https://doi.org/10.1007/s42947-021-00088-0.

[31] A. Kavussi, S.M. Motevalizadeh, Exploring the role of extreme thermal conditions and freeze–thaw cycling on crack growth resistance of WMA mixes: an analytical and statistical analysis, Int. J. Pavement Eng. (2021), https://doi.org/10.1080/10298436.2021.2011871.
[32] A. Kavussi, M. Motevalizadeh, A. Karimi, A. Rahimizadeh, Evaluating the Moisture Resistance of Foam Warm Mix Asphalt Using Image Processing Method, 03 (2017) 1–7.
[33] A. Gundla, S. Underwood, Evaluation of in situ RAP binder interaction in asphalt mastics using micromechanical models, Int. J. Pavement Eng. 18 (2017) 798–810, https://doi.org/10.1080/10298436.2015.1066003.
[34] J. Mirwald, D. Nura, B. Hofko, Recommendations for handling bitumen prior to FTIR spectroscopy, Mater. Struct. Constr. 55 (2022), https://doi.org/10.1617/s11527-022-01884-1.
[35] S.M. Motevalizadeh, K. Mollenhauer, J. Wetekam, FTIR spectroscopy and multivariate discriminant analysis for classifying bituminous mastics: exploring aging states and mastic composition, Constr. Build. Mater. 438 (2024), https://doi.org/10.1016/j.conbuildmat.2024.137188.
[36] D. Dalmazzo, A. Jiménez Del Barco Carrión, L. Tsantilis, D. Lo Presti, E. Santagata, Non- petroleum- based binders for paving applications: Rheological and chemical investigation on ageing effects, in: Proc. 5th Int. Symp. Asph. Pavements Environ., Padova, Italy, 2019: pp. 67–76. https://doi.org/10.1007/978-3-030-29779-4_7.
[37] M. van Gurp, J. Palmen, Time-temperature superposition for polymeric blends, J. Rheol. Bull. 65 (1998) 5–8.
[38] X. Liu, M. Zhang, L. Shao, Z. Chen, Effect of volcanic ash filler on thermal viscoelastic property of SBS modified asphalt mastic, Constr. Build. Mater. 190 (2018) 495–507, https://doi.org/10.1016/j.conbuildmat.2018.09.101.
[39] C.V. Phan, H. Di Benedetto, C. Sauzéat, D. Lesueur, Influence of hydrated lime on linear viscoelastic properties of bituminous mixtures, RILEM Book. 11 (2016) 667–680, https://doi.org/10.1007/978-94-017-7342-3_54.
[40] B. Hofko, M.Z. Alavi, H. Grothe, D. Jones, J. Harvey, Repeatability and sensitivity of FTIR ATR spectral analysis methods for bituminous binders, Mater. Struct. Constr. 50 (2017), https://doi.org/10.1617/s11527-017-1059-x.
[41] A. Margaritis, H. Soenen, E. Fransen, G. Pipintakos, G. Jacobs, J. Blom, W. Van den bergh, Identification of ageing state clusters of reclaimed asphalt binders using principal component analysis (PCA) and hierarchical cluster analysis (HCA) based on chemo-rheological parameters, Constr. Build. Mater. 244 (2020), https://doi.org/10.1016/j.conbuildmat.2020.118276.
[42] S.M. Motevalizadeh, A. Kavussi, K. Mollenhauer, Predicting the fracture mechanics responses of recycled asphalt mixes using machine learning-based algorithms: application of CART algorithm and neural networks, Eng. Fract. Mech. 276 (2022), https://doi.org/10.1016/j.engfracmech.2022.108791.